Lab on a Chip

Cite this: *Lab Chip*, 2012, **12**, 2843–2849

www.rsc.org/loc

PAPER

Automated analysis of single stem cells in microfluidic traps†

Stefan A. Kobel,[a] Olivier Burri,[b] Alexandra Griffa,[bc] Mukul Girotra,[a] Arne Seitz[b] and Matthias P. Lutolf*[a]

Received 2nd April 2012, Accepted 19th April 2012
DOI: 10.1039/c2lc40317j

We report a reliable strategy to perform automated image cytometry of single (non-adherent) stem cells captured in microfluidic traps. The method rapidly segments images of an entire microfluidic chip based on the detection of horizontal edges of microfluidic channels, from where the position of the trapped cells can be derived and the trapped cells identified with very high precision (>97%). We used this method to successfully quantify the efficiency and spatial distribution of single-cell loading of a microfluidic chip comprised of 2048 single-cell traps. Furthermore, cytometric analysis of trapped primary hematopoietic stem cells (HSC) faithfully recapitulated the distribution of cells in the G1 and S/G2-M phase of the cell cycle that was measured by flow cytometry. This approach should be applicable to automatically track single live cells in a wealth of microfluidic systems.

Introduction

In population-based *in vitro* assays, the behaviour of single cells is masked. This can be a major problem in the study of heterogeneous populations of mammalian cells such as primary stem cells or tumor cells, whose proliferative and differentiation capacity can fluctuate significantly at single cell level.[1,2] To address this problem, single cell analysis platforms have been developed that rely on the use of micro-scale technologies to handle single cells in high-throughput[3–5] or on the miniaturization and parallelization of flow cytometry.[6]

Cells in such micro-devices are typically imaged using microscopes or scanners and information on their behavior requires challenging image analysis. First, these platforms typically span over more than one single field of view, resulting in large surfaces to be imaged contiguously and dynamically over many days. Moreover, equivalent microstructures and cells are often densely packed and thus appear many times in a single image.[7–9] The resulting large image stacks must be correctly segmented and annotated. Secondly, the cells have to be reliably identified in segmented images.[8,9] This task is ideally performed in brightfield and non-fluorescent images, in order to leave fluorescence channels open for cell analysis. Finally, a fluorescence-based approach can be biased because brighter cells are preferentially detected or their size is over-estimated.[10]

To cope with these issues, researchers have developed algorithms to semi-automatically derive the position of the microstructures and to identify cells on the chip. These algorithms are either based on a manual alignment of segmentation masks followed by an automated analysis,[8,11,12] or on computationally intensive image de-convolution.[9] Alternatively, fluorescently-labelled cells are first detected and, based on the position of cells, the structure of the microfluidic chip is inferred.[13,14] However, with few exceptions,[8,9] a rigorous assessment of the performance of segmentation methods has not been performed.

Here we report a detailed description and validation of an automated image cytometry approach applied to a microfluidic device consisting of 2048 arrayed single-cell traps. We developed image-processing algorithms to segment images of the entire microfluidic chip into cropped regions containing only the area of the single-cell trap, and thus efficiently identified trapped cells. This approach allowed quantifying the spatial distribution of single-cell trapping on the microfluidic chip, automatic tracking of dividing hematopoietic stem cells (HSC) at single cell level and over several hours, as well as the high-throughput detection of cell cycle phases in individual HSCs.

Materials and methods

Fabrication and operation of the microfluidic chip

Microfluidic chips were fabricated by multi-layered soft-lithography in poly(dimethylsiloxane) (PDMS).[7,15,16] They consisted of single-cell traps[17] that were grouped serially in units of eight traps, which were arranged in a parallel manner, forming an array of 2048 single-cell traps distributed over eight columns (Fig. 1). Cells were loaded at a flow rate of 50–100 nL min^{-1}

[a]*Laboratory of Stem Cell Bioengineering (LSCB), Institute of Bioengineering and School of Life Sciences, Ecole Polytechnique Fédérale de Lausanne (EPFL), CH-1015, Lausanne, Switzerland. E-mail: matthias.lutolf@epfl.ch; Tel: +41 (0) 21693 1876*
[b]*BioImaging and Optics Core Facility, Ecole Polytechnique Fédérale de Lausanne (EPFL), CH-1015, Lausanne, Switzerland*
[c]*Signal Processing Laboratory 5, Ecole Polytechnique Fédérale de Lausanne (EPFL), CH-1015, Lausanne, Switzerland*

† Electronic Supplementary Information (ESI) available: Fig. S1: Pseudo-code describing the presented algorithm. Fig. S2: Example of parameters used to detect the single-cell traps. Fig. S3: Automated detection and correction of missed and mislabeled segments. Fig. S4: Use of different pixel statistics to detect single cells. Fig. S5: Systematic testing of different thresholding algorithms to detect single cells. Fig. S6: Size distribtion of trapped cells. See DOI: 10.1039/c2lc40317j

onto the microfluidic chip using syringe pumps and maintained in the trap by a constant perfusion of 10 nL min^{-1}. Experiments were performed under a humidified atmosphere and 5% CO_2.

The microfluidic chip was imaged using an automated microscope (Zeiss Observer Z1, Zeiss, Germany) with an integrated incubator at 10× magnification using a CoolSnap ES2 CCD camera (Photometrics, USA). The microscope was controlled by MetaMorph (Visitron, Germany), a multifunctional imaging software that allows the generation of stitched images using a built-in scan slide option. To this end, the chip was first aligned to the microscope such that the columns of traps were in line with the long side of the camera of the microscope. The microscope was then programmed to scan the eight areas where the single cell traps were located, to focus using the built-in auto-focus algorithm and to produce assembled images of these areas that were overlapping by approximately 10%. The images were then stitched by using the "stitch grid of image" option of Fiji,[18] a distribution of the image processing software ImageJ that was optimized for biological images analyses (http://fiji.sc/wiki/index.php/Fiji). The stitching was performed without computationally optimizing the overlap, because this option performed a cross-correlation of the images and sometimes skipped or repeated single traps in the stitched images.

Image segmentation to detect single-cell traps

The algorithm to segment the microfluidic single-cell traps ("μ-TrapFinder") was written in MatlabTM (Version 7, release 14, MathWorks) and is summarized as pseudo-code in Fig. S1, ESI†. Briefly, the images were first rotated to align the chip along the horizontal axis. In order to detect horizontal edges that are characteristic for the position of the single-cell trap, the images were filtered using a Sobel filter (Fig. S2†). The filtered images were then thresholded and the identified objects were sorted by their x-position. Dust particles were excluded from the analysis-based morphological criteria. In addition, non-detected lines were identified and completed by interpolation from the position of the neighboring traps (Fig. S3†). To threshold the images, we applied an "Otsu" threshold.[19]

Next, the position of the trap was calculated relative to the center of the identified lines and locally refined by aligning the segmentation mask to neighboring vertical lines. Finally, the image of the microfluidic chip was segmented and the resulting images saved as TIFF stacks in which each slice contained the

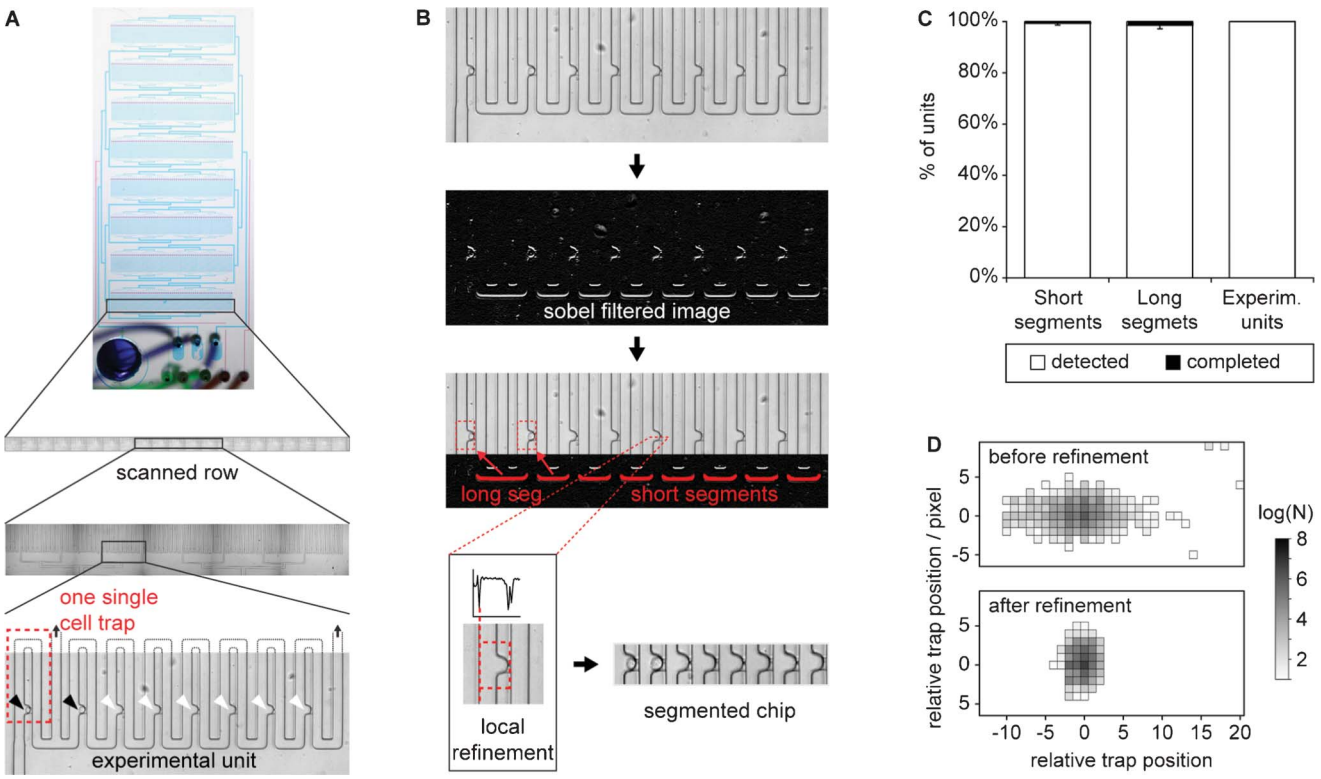

Fig. 1 Image-based cytometry on a microfluidic chip. (A) The microfluidic chip consists of eight rows of microfluidic single-cell traps that are scanned, yielding stitched images of 21 positions. Each row of the chip comprises 32 experimental units with eight microfluidic single-cell traps that hydrodynamically capture single cells in small cavities.[17] The entire chip consists of 2048 single-cell traps. Full or empty traps are labelled with a black or white arrowhead, respectively. (B) To detect single-cell traps, the chip is Sobel-filtered, revealing the edges of horizontal channels. Since some of these edges are denotative for the position of the single-cell traps, the identified edges are filtered according to their length, thickness and position and non-detected elements are completed. The length of the detected lines allows a distinction between the first trap and the subsequent ones in an experimental unit. After refining the lateral position of the mask based on local minima of a line scan, the stitched image is segmented and the cropped images are exported. (C) The detection of short and long segments is very reliable. (D) Measurements of the relative position of the single-cell traps in the cropped images reveals a high spatial precision of the image cropping. The local refinement step described in (B) can further improve the precision. All data are from 3 different chips and more than 6000 single-cell traps.

eight traps of an experimental unit. All steps were performed automatically and required no fine-tuning, except for entering the geometrical properties of the chip. The process can also be batched very easily.

Measurement of image segmentation precision

To assess the spatial precision by which the microfluidic chip was segmented, the centers of the microfluidic single-cell trap were estimated in the stacks with the segmented images of the empty chips. To this end, we measured the intensity profile along horizontal and vertical lines through the trap in Fiji. The minima of these profiles or geometric center of the two minima, respectively, were used as the x- and y-position of the trap.

Isolation of primary HSCs

HSCs were isolated from the bone marrow of 8–12-week-old C57BL/6 mice, stained and purified as previously described.[20,21] In brief, after flushing out the bone marrows cells, red blood cells were lysed (RBC lysis buffer, eBioScience, Switzerland) and differentiated cells were magnetically labeled using a lineage depletion kit (BD Bioscience) and removed from the sample using a MidiMACS magnetic column (Miltenyi Biotech, Germany). Cells were then stained with anti-c-Kit-PE/Cy7 and anti-Sca1-PE (eBioScience, Switzerland) and separated by FACS on a BD Aria instrument (BD Bioscience, USA) at the EPFL FACS core facility. Single viable (propidium iodide negative) $Lin^{-}ckit^{+}$ $Sca1^{+}$ $CD150^{+}$ cells were double-sorted. All animal experiments were conducted in compliance with the law and the internal guidelines of EPFL.

Transfection of HSCs with FUCCI reporters

After isolation and purification, HSCs were transferred into StemLine II (Sigma) medium supplemented with 100 ng ml^{-1} SCF and 2 ng ml^{-1} Flt-3 ligand, and incubated with the two vectors for the "Fluorescence Ubiquitination Cell Cycle Indicator" (FUCCI) system at a multiplicity of infection (MOI) of 250. After over-night incubation, the cells were washed twice and cultured for additional four days to allow the signal of the FUCCI reporters to come up before loading them on-chip.

Automated single cell detection and analysis

To detect trapped single cells, we tested defocusing, various pixel statistics (Fig. S4†) and the thresholding algorithms that are provided by Fiji. These algorithms can automatically threshold images based on their intensity histograms (see http://www.fiji.sc/ for more details). In brief, the cropped images of the single-cell traps that had been acquired at different focus positions were processed individually as 8-bit images, optionally treated with a Mexican hat filter (also known as Laplacian of Gaussian, LoG),[22] and then thresholded using the different algorithms provided by Fiji. The resulting binary images were eroded to avoid the detection of microstructures and the microstructures masked in the thresholded image (Fig. 2A). The cells were detected using a 4-connected particle detector for ImageJ (http://www.dentistry.bham.ac.uk/landinig/software/software.html). Images of traps that were off-focus or

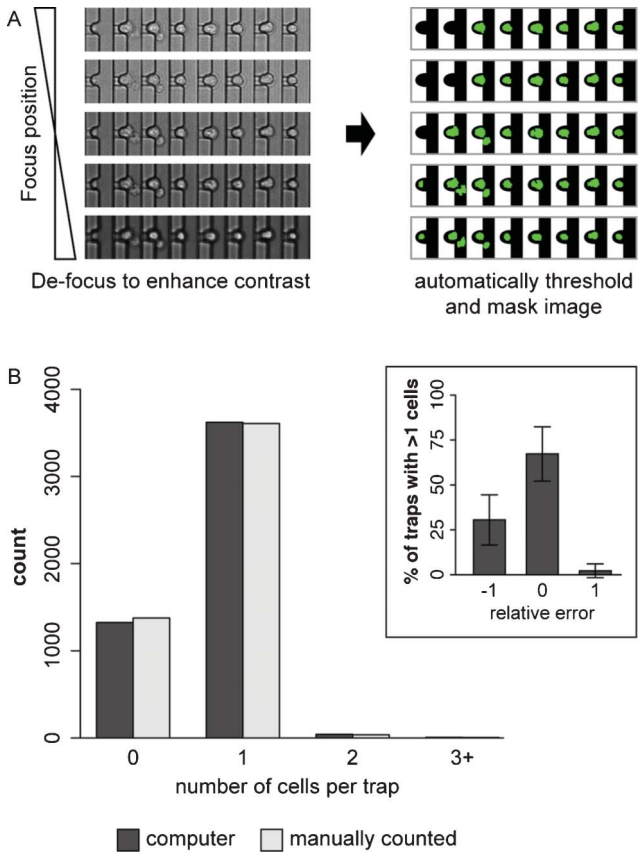

Fig. 2 Automated detection of single cells in microfluidic chips. (A) In order to detect cells in traps, images were acquired at different focal planes and then thresholded. In the binary images, non-cellular structures were removed with a mask (in light gray) and the cells identified (green). (B) Using this approach, cells are efficiently identified in the single-cell traps (sum from three chips). However, cells are detected less efficiently when there is exceptionally more than one cell per trap (insert).

contained dust particles or cell debris were excluded from the analysis.

To analyze cells on the microfluidic chip, de-focused images (+8 μm) and a "Triangle" thresholding algorithm were used. This algorithm is part of the Fiji distribution and is a geometric method that automatically thresholds images based on their intensity histogram. The algorithm recovers the maximum distance between the histogram and the segment joining the peak and maximum intensity of the histogram. The intersection of this maximum with the histogram (plus an offset of 20% of the maximum intensity) defined the threshold.[23] The mask that was obtained with the "Triangle" thresholding algorithm was used to measure their fluorescence signal. These masks were also used to determine the surface of the detected cells.

Statistical analysis

To assess the performance of our algorithms, the computed results were compared to manually counted data. Statistical analyses were performed using the R package (http://www.r-project.org/). All experiments were performed in triplicate and, unless noted otherwise, results were represented as means with the standard deviation.

Results

Operation and imaging of the microfluidic chip

The design of the microfluidic chip is based on our previously published microfluidic single-cell trap system (Fig. 1).[17] A trap consists of a long looped main channel, a cavity for a single cell and a three μm-high gap that connects the cavity to the exit of the main channel (Fig. 1A). Media flow drags cells into the trap and stably maintains it there. In accordance with our previous data, loaded HSCs were efficiently trapped and more than 90% of single-cell traps could be filled.

To facilitate imaging, the chip was spatially aligned to the microscope such that 21 positions were sufficient to cover a row of microfluidic cell traps, resulting in approximately 13 traps per image. Since each column was imaged using a scanning option, these 21 images were acquired relative to the eight starting positions (*i.e.* the first trap of a row). Of note, although manually defined, these starting positions and all subsequent images could be defined with a high spatial resolution. As a consequence, this semi-automated approach led to homogeneous scans where the positions of the microfluidic channels varied usually less than 200 μm between different images.

Detection and cropping of individual single-cell traps

In these standardized image sets (Fig. 1A), the micro-structured single-cell traps were detected. An image was first aligned automatically to the horizontal and then filtered to detect horizontal edges (Fig. 1B). The horizontal elements were denotative for the position of the single-cell traps: long lines with a length of 105 pixels indicated the presence of a first trap in an experimental unit and 65 pixel-long lines for the subsequent traps (Fig. 1B and Fig. S2†). Dust particles and off-focus information could be reliably excluded from the analysis by their length (with tolerance for the short or long segments of ± 10 pixels and ± 20 pixels, respectively), their height (less than 20 pixels) or the *y*-position. Together, these criteria were sufficient to identify more than 98% ($\pm 1\%$, $n = 3$) of the long segments and 99.2% ($\pm 0.6\%$) of the short segments (Fig. 1C).

The identified segments gave a framework to calculate the position of the few non-detected segments (Fig. S3†). Due to the known geometry of the chip, we reliably calculated the position of all 2048 single cell traps, and after an additional sorting and annotation step, we also correctly assembled all the experimental units (Fig. 1C). The number of incorrectly detected units was less than 0.5% per chip ($n = 3$).

Next, we determined the spatial precision of the image segmentation and whether this precision could be improved by refining the position of the crop mask based on local features of the microfluidic chip (Fig. 1B). We therefore assessed the relative position of the main channels and the trap cavity in the cropped images and found that the images were segmented precisely. The position of the trap in cropped images varied only by 2.4 pixel in *x* and 0.74 pixel in *y* (determined as the standard deviation of the relative position of the trap in the cropped images, $n = 3$). Furthermore, the segmentation accuracy along the *x*-axis could be further improved to approximately 0.6 pixels with a local refinement step (Fig. 1D).

Of note, the detection of the microfluidic structures and the subsequent cropping is very fast. On a normal 64 bit work station equipped with a Pentium i7 processor (3.5 GHz, 32 GB RAM), one scan with 21 images can be processed within 30 seconds, of which only about 10 seconds are required to detect the traps. The remaining time is due to file handling and image rotation at the beginning of the analysis. Accordingly, an entire chip can be processed in less than 4 minutes.

Automated segmentation of trapped cells

After obtaining cropped images of the single-cell traps, we sought to exploit statistical analyses of the trap region to detect occupied or empty traps (Fig. 2A and Fig. S4†). Indeed, simple pixel statistics, such as the maximum, mean and the standard deviation of the pixel intensities in the trap area were sufficient to discriminate between empty and filled traps (Fig. S4†). In particular, when the images were acquired with a strong defocus,[10] the cells were detected with a sensitivity of up to 95% and a specificity of up to 99% (Fig. S4†). Interestingly, while the standard deviation and maximum intensities were most predictive for larger measurement areas, the mean of the pixel intensities was most precise when only a few pixels were considered in the analysis (Fig. S4†).

In order to measure other properties of trapped cells, such as their size or a fluorescent signal, we systematically tested different thresholding algorithms provided by Fiji at different focus positions and we also applied a LoG filter to enhance bright spots.[22] When compared with manually counted data, many of the tested combinations were very sensitive (>90%) and specific (97%, Fig. S5†). Thus we were able to correctly measure the number of cells per trap (Fig. 2B). However, in rare cases where traps were filled with more than one cell, we also compared whether the thresholding algorithms detected the correct number of cells (Fig. 2B, insert). These experiments showed that in more than 65% of events multiple cells were correctly detected, while 30% could not detect the second cell.

Assessing single-cell dynamics on microfluidic chips

As a first application of the method, we assessed the distribution of HSCs in the experimental units upon loading of the microfluidic chip. When the chip was loaded only with 1000 cells, the trap occupancy decreased nearly linearly through the experimental units. The first traps in the experimental units were preferentially loaded with cells, while the last traps were mostly empty (Fig. 3A). In contrast, when the chip was loaded with about 2000 cells, almost all the traps in the experimental units were occupied (Fig. 3A). The size of the trapped cells was 42.6 (± 0.3) μm^2 ($n = 3$) (Fig. S6†).

In contrast to the analysis of single cells by flow cytometry, microfluidic chips offer the advantage of tracking single cells over multiple time points.[11,14,17] We demonstrate this capability by loading only a few cells onto our microfluidic chip and then repeatedly imaging them (see supplementary movie 1†). Our algorithm can correctly detect single HSCs in these time-lapse movies, even after HSC divisions as shown in an example of Fig. 3B.

Cytometric analysis to detect cell cycle phases in single HSCs

One of the major applications of cytometry is the measurement of fluorescent signals from single cells, for example to probe

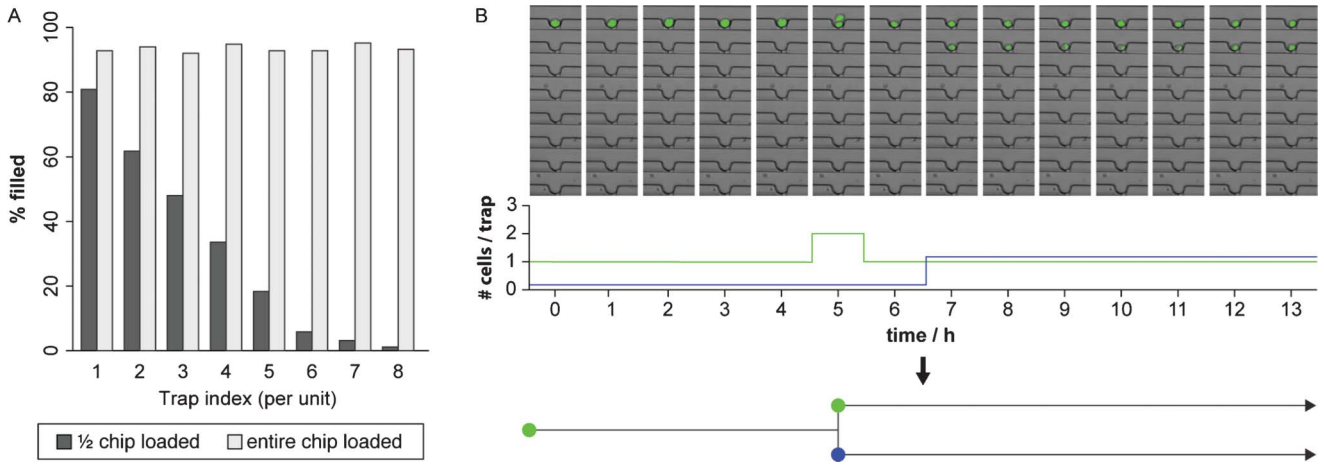

Fig. 3 Assessing single-cell dynamics on microfluidic chips. (A) Cell distribution in the experimental units of a partially loaded (approximately 1000 cells loaded in 2048 traps) and fully loaded microfluidic chip. The occupancy of single-cell traps declines with the distance from the first trap in a half loaded chip. (B) Example of automated tracking of a dividing HSC. Since the microfluidic chip is perfused, the daughter cells are physically separated by the perfusion after division.[17] Our algorithm is able to correctly track this event.

viability or to detect the expression of a particular reporter gene. Here we focused on determining cell cycle phases of individual HSCs, since this parameter is an important indicator of the stem cell state. That is to say, *in vivo* most long-term repopulating HSCs are quiescent, *i.e.* in the G0 phase of the cell cycle.[24] We employed the FUCCI system which reports the cell cycle phase in single cells by red (G1 or G0) and green (S/G2-M) fluorescent reporters that are fused to the cell cycle regulators Cdt1 and geminin, respectively.[25]

The two FUCCI reporters can be well detected on our chip and we obtained *ca.* 12.8 (±2.3)% of HSCs in S/G2-M and 10.5 (±3.0)% in G1 (Fig. 4). A small fraction of cells (0.93 ± 0.6%) were positive for both markers, indicating that they were in the transition from G1 to S. The majority of HSCs were neither green nor red, because the transduction efficiency was low.

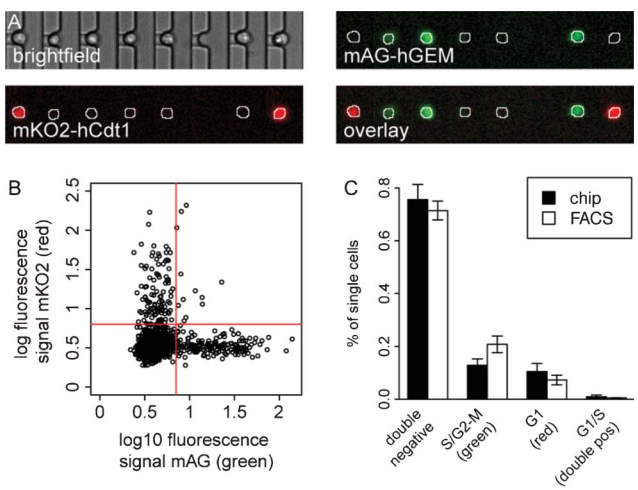

Fig. 4 Cytometric analysis of FUCCI-HSCs. (A) Micrographs of trapped HSCs that were transfected with fluorescent reporters to mark S/G2-M (green) and G1 (red) and that were detected by the presented algorithm (white masks). (B) Example of plot showing the populations of green and red HSCs on the microfluidic chip. (C) Comparison of image and flow cytometry for the analysis of the cell cycle phases.

Compared to flow cytometry, our image cytometry approach correctly estimated the number of cells in G1 (red) and the transition from G1 to S (double-positive), but somewhat underestimated the number of cells in S/G2-M (green) ($p < 0.05$).

Discussion

Although there are versatile platforms to detect alignment marks on microfluidic chips (*e.g.* IMAQ from National Instruments[26]) or image analysis programs to segment single cells (*e.g.* ImageJ[27,28] or Cell Profiler[29]), none of these systems is yet able to automatically distinguish and annotate both single cells and microstructures in microfluidic chips. Since most microfluidic chips are fabricated from elastic and rather soft PDMS, their microstructures often contain local distortions. These deviations from the ideal geometry impede the use of a few global alignment markers,[26] as are often used in the semi-conductor fabrication[30] or sometimes in microarray analysis.[8,11,12] For this reason, a chip must contain regularly spaced markers[26] or microstructures of a micro-device can directly serve as fiducials that can be discovered by template matching.[9] We tested this method by using various deconvolution masks (data not shown) but found that it was not possible to distinguish the single-cell trap from the other micro-channels. We therefore adapted automated edge detection, normally used for the detection of global alignment marks,[30] to detect local characteristic structures on our chip. While global alignment marks are isolated from other structures, our fiducials were surrounded by many other elements of the densely packed chip. In order to reliably distinguish the fiducials from other microstructures, we employed a directional Sobel filter, simple morphological criteria and the known geometry of the chip. In a second step, the exact positions of the single-cell traps were deduced from these characteristic segments. This approach was fast and resulted in perfectly segmented and annotated chips (Fig. 1C). In addition, the spatial precision was very high, albeit slightly reduced in x (Fig. 1D). To compensate for this reduced precision, we integrated a local refinement step, such that more than 95% of traps were segmented with a precision of less than

1 pixel (trap diameter *ca*. 15 pixels). The refinement step also helped to correct local distortions of the chip that may occur due to manual fabrication. This would not be possible by aligning a global crop mask.[26]

Our image segmentation was based on standardized, stitched images of the microfluidic chip. Although such coherent images are not a prerequisite for successful image segmentation, we found that stitched images facilitated the identification of outliers and non-detected microstructures. For example, when only a few traps were detected, the chip was still correctly annotated based on information from neighbouring images. It should also be noted that our approach requires straight lines to detect micro-features and will probably not work on round shapes such as microwell arrays. However, since most microfluidic chips contain straight features[11,14] or can be equipped with regularly shaped position markers,[12,31] we are confident that the algorithm can be adapted to detect microstructures on most microfluidic devices.

Due to the very good accuracy in determine the position of trapped cells on the microfluidic chip, it was relatively straightforward to identify trapped single stem cells. For example, a statistical description of the pixel intensities in the trap area was sufficient to identify single cells very precisely (Fig. S4†). However, since this approach would only indicate whether a cell is present or not, but not allow any additional analyses (*e.g.* on cell size, fluorescence, *etc.*), we did not pursue this strategy further. Instead, we used an automated and user-unbiased thresholding algorithm to detect cells in the microfluidic traps. Our systematic tests demonstrated that automated thresholding can be similarly sensitive and specific as the statistical analysis described above (Fig. S5†), and it can assess the number of cells per single-cell trap (Fig. 2B). Interestingly, some of the tested thresholding algorithms were less efficient in detecting cells when used on below-focus (−8 μm, −4 μm) and in-focus images (Fig. S5A†), likely because cells tend to appear brighter when imaged above-focus. As a consequence, cells were more easily detected.[10]

These findings can also partially explain why the detection of multiple cells posed a hurdle to some thresholding algorithms. Either the cells were not segmented properly or, when they were segmented, the second cell was not detected because the geometry of the microfluidic trap immobilized the cells at the bottom of the microfluidic chip.[17] Additional cells in the trap were mostly in the centre of the channel (Fig. 2A). This difference in focal position most probably explains why the two cells in the microfluidic chip were detected with different efficiencies (Fig. 2D).

Notwithstanding these open issues, our algorithm performed generally better compared to most other methods[8,9] and we were able to precisely quantify the efficiency and spatial distribution of single-cell loading of a microfluidic chip (Fig. 3A) or to track single cell divisions in microfluidic chips (Fig. 3B).

As a proof-of-concept application, we loaded FUCCI-HSCs onto the chip and analyzed their cell cycle phases (Fig. 4). Compared to flow cytometry, the difference between stem cells in G1 (red cells) and the transition from G1 to S (orange cells) was correctly measured, but the fraction of cells in S/G2-M (green) somewhat underestimated. This error might be due to the smaller linear dynamic range of microscopes compared to flow cytometers, a problem that could be overcome with a higher numerical aperture.

Conclusion

Micro-devices are becoming more and more widely used for the analysis of single cells. This also increases the need for reliable methods to detect single cells. Here we report a quantitative description of such an image analysis approach and demonstrate that images of microfluidic single-cell traps can be segmented with sub-pixel accuracy and without cropping important cellular information. The method can be easily adapted to other microfluidic chips. To prove the potential of combining image cytometry and microfluidic single-cell trapping, we automatically assessed the efficiency of cell handling, tracked single cell divisions on-chip and successfully detected fluorescence signals from single cells. This approach should afford on-chip cytometry of diverse single-cell behaviors in long-term microfluidic cultures.

Acknowledgements

The authors thank Dr Marta Roccio for support in establishing the FUCCI system in the lab.

References

1 D. G. Spiller, C. D. Wood, D. A. Rand and M. R. White, *Nature*, 2010, **465**, 736–745.
2 T. Schroeder, *Nature*, 2008, **453**, 345–351.
3 J. El-Ali, P. K. Sorger and K. F. Jensen, *Nature*, 2006, **442**, 403–411.
4 S. Kobel and M. P. Lutolf, *BioTechniques*, 2010, **48**, IX–XXII.
5 D. Wang and S. Bodovitz, *Trends Biotechnol.*, 2010, **28**, 281–290.
6 B. McKenna, J. G. Evans, M. C. Cheung and D. Ehrlich, *Nat. Methods*, 2011, **8**, 401–403.
7 T. Thorsen, S. J. Maerkl, S. R. Quake, *Science* (New York, NY) 2002, **298**, pp. 580–584.
8 V. Lecault, M. Vaninsberghe, S. Sekulovic, D. J. Knapp, S. Wohrer, W. Bowden, F. Viel, T. McLaughlin, A. Jarandehei, M. M. Miller, D. Falconnet, A. K. White, D. G. Kent, M. R. Copley, F. Taghipour, C. J. Eaves, R. K. Humphries, J. M. Piret and C. L. Hansen, *Nat. Methods*, 2011, **8**(7), 581–586.
9 N. Kachouie, L. Kang and A. Khademhosseini, *BioTechniques*, 2009, **47**, x–xvi.
10 A. Gordon, A. Colman-Lerner, T. E. Chin, K. R. Benjamin, R. C. Yu and R. Brent, *Nat. Methods*, 2007, **4**, 175–181.
11 D. Di Carlo, N. Aghdam and L. P. Lee, *Anal. Chem.*, 2006, **78**, 4925–4930.
12 K. Roach, K. R. King, B. Uygun, I. Kohane, M. L. Yarmush and M. Toner, *Biotechnology progress*, 2009, **25**, 1772–1779.
13 K. Chung, C. A. Rivet, M. L. Kemp and H. Lu, *Anal. Chem.*, 2011, **83**(18), 7044–7052.
14 S. Faley, K. Seale, J. Hughey, D. K. Schaffer, S. VanCompernolle, B. McKinney, F. Baudenbacher, D. Unutmaz and J. P. Wikswo, *Lab Chip*, 2008, **8**, 1700–1712.
15 S. J. Maerkl, S. R. Quake, *Science* (New York, NY) 2007, **315**, pp. 233–237..
16 Y. N. Xia and G. M. Whitesides, *Annu. Rev. Mater. Sci.*, 1998, **28**, 153–184.
17 S. Kobel, A. Valero, J. Latt, P. Renaud and M. Lutolf, *Lab Chip*, 2010, **10**, 857–863.
18 S. Preibisch, S. Saalfeld, P. Tomancak, *Bioinformatics* (Oxford, England) 2009, **25**, pp. 1463–1465..
19 N. Otsu, *IEEE Trans. Syst. Man Cybern.*, 1979, **9**, 62–66.
20 M. P. Lutolf, R. Doyonnas, K. Havenstrite, K. Koleckar and H. M. Blau, *Integr. Biol.*, 2009, **1**, 59–69.
21 S. Kobel, M. Limacher, S. Gobaa, T. Laroche and M. P. Lutolf, *Langmuir*, 2009, **25**, 8774–8779.
22 D. Sage, F. R. Neumann, F. Hediger, S. M. Gasser and M. Unser, *IEEE transactionson image processing: a publication of the IEEE Signal Processing Society*, 2005, **14**, 1372–1383.
23 G. W. Zack, W. E. Rogers and S. A. Latt, *J. Histochem. Cytochem.*, 1977, **25**, 741–753.

24 A. Wilson, E. Laurenti, G. Oser, R. C. van der Wath, W. Blanco-Bose, M. Jaworski, S. Offner, C. F. Dunant, L. Eshkind, E. Bockamp, P. Lió, H. R. Macdonald and A. Trumpp, *Cell*, 2008, **135**, 1118–1129.
25 A. Sakaue-Sawano, H. Kurokawa, T. Morimura, A. Hanyu, H. Hama, H. Osawa, S. Kashiwagi, K. Fukami, T. Miyata, H. Miyoshi, T. Imamura, M. Ogawa, H. Masai and A. Miyawaki, *Cell*, 2008, **132**, 487–498.
26 J. Huft, D. J. Da Costa, D. Walker and C. L. Hansen, *Lab Chip*, 2010, **10**, 2358–2365.
27 T. J. Collins, *BioTechniques*, 2007, **43**, 25–30.
28 S. G. Megason and S. E. Fraser, *Cell*, 2007, **130**, 784–795.
29 A. E. Carpenter, T. R. Jones, M. R. Lamprecht, C. Clarke, I. H. Kang, O. Friman, D. A. Guertin, J. H. Chang, R. A. Lindquist, J. Moffat, P. Golland and D. M. Sabatini, *GenomeBiology*, 2006, **7**(10), R100 Epub 2006 Oct 31.
30 L. Chorng-Tyan and Y. Yuan-Chen, *Mechatronics, 2005. ICM '05. IEEE International Conference on*, **2005**, 762–767.
31 A. Ogunniyi, C. Story, E. Papa, E. Guillen and J. Love, *Nat. Protoc.*, 2009, **4**, 767–782.